Geophysical Journal International

Geophys. J. Int. (2023) **233,** 234–252
Advance Access publication 2022 November 22
GJI Marine Geosciences and Applied Geophysics

https://doi.org/10.1093/gji/ggac461

Frequency-dependent AVO inversion applied to physically based models for seismic attenuation

Nisar Ahmed [1], Wiktor Waldemar Weibull [1], Beatriz Quintal [2], Dario Grana [3] and Tuhin Bhakta [4]

[1] *Department of Energy Resources, University of Stavanger,* 4021 *Stavanger, Norway. E-mail: nisar.ahmed@uis.no*
[2] *Institute of Earth Sciences, University of Lausanne,* 1015 *Lausanne, Switzerland*
[3] *Department of Geology and Geophysics, School of Energy Resources, University of Wyoming, Laramie, Wyoming* 82071*, USA*
[4] *NORCE Norwegian Research Centre, Nygårdsgaten* 112, 5008 *Bergen, Norway*

Accepted 2022 November 15. Received 2022 September 16; in original form 2022 July 18

SUMMARY

Seismic inversion of amplitude versus offset (AVO) data in viscoelastic media can potentially provide high-resolution subsurface models of seismic velocities and attenuation from offset/angle seismic gathers. *P*- and *S*-wave quality factors (Q), whose inverse represent a measure of attenuation, depend on reservoir rock and pore fluid properties, in particular, saturation, permeability, porosity, fluid viscosity and lithology; however, these quality factors are rarely taken into account in seismic AVO inversion. For this reason, in this work, we aim to integrate quality factors derived from physically based models in AVO inversion by proposing a gradient descent optimization-based inversion technique to predict the unknown model properties (*P*- and *S*-wave velocities, the related quality factors and density). The proposed inversion minimizes the non-linear least-squares misfit with the observed data. The optimal solution is iteratively obtained by optimizing the data misfit using a second-order limited-memory quasi-Newton technique. The forward model is performed in the frequency–frequency-angle domain based on a convolution of broad-band signals and a linearized viscoelastic frequency-dependent AVO (FAVO) equation. The optimization includes the adjoint-state-based gradients with the Lagrangian formulation to improve the efficiency of the non-linear seismic FAVO inversion process. The inversion is tested on synthetic seismic data, in 1-D and 2-D, with and without noise. The sensitivity for seismic quality factors is evaluated using various rock physics models for seismic attenuation and quality factors. The results demonstrate that the proposed inversion method reliably retrieves the unknown elastic and an-elastic properties with good convergence and accuracy. The stability of the inverse solution especially seismic quality factors estimation relies on the noise level of the seismic data. We further investigate the uncertainty of the solution as a function of the variability of the initial models.

Key words: Inverse theory; Joint inversion; Numerical modelling; Seismic attenuation; Rock physics and AVO inversion; Marine geosciences and applied geophysics.

1 INTRODUCTION

Seismic waves propagation through the geological layers leads to the amplitude loss of coherent wave front due to absorption and transmission caused by numerous elastic and an-elastic subsurface mechanisms (Kneib & Shapiro 1995; Wang 2019). The energy absorption effect also referred to as seismic attenuation, is measured by the inverse of the quality factor (Q), which can thus be estimated, for example, from the amplitude decay of seismic waves. The energy loss might depends on the heterogeneity of rock and pore fluid properties which can cause both scattering and wave-induced fluid flow (White 1975; Pride & Berryman 2003a, b; Pride *et al.* 2004; Carcione & Picotti 2006; Tisato & Quintal 2013; Caspari *et al.* 2019; Mavko *et al.* 2020; Chapman *et al.* 2021). Seismic wave attenuation caused by such physically based mechanisms is frequency dependent and can be approximated by a viscoelastic model (Jänicke *et al.* 2015, 2019).

At a geological horizon between two viscoelastic interfaces, the seismic reflection amplitude variations depend on the *P*- and *S*-wave quality factors together with *P*- and *S*-wave velocities and density (Innanen 2011; Zhao *et al.* 2014; Li & Liu 2019). In viscoelastic media,

seismic waves exhibit dispersion and thereby the magnitude of reflection amplitudes is not only dependent on the medium properties and incident angles but are also strongly affected by the frequency (Chapman *et al.* 2006; Jin *et al.* 2017; Kumar *et al.* 2020). Therefore, the estimation of both seismic quality factors along with elastic properties can give valuable information regarding the Earth's subsurface properties, such as temperature, pressure, lithology and fluid content (Peters *et al.* 2012; Cheng 2013; Sheehan *et al.* 2014; Zong *et al.* 2015; Chen *et al.* 2018; Li & Liu 2019). Numerous studies (Pride *et al.* 2004; Carcione 2007; Tisato & Quintal 2013; Chapman *et al.* 2021) have shown that the wave-induced fluid flow (WIFF) is the dominant source of seismic waves attenuation in partially fluid-saturated sediments in the seismic frequencies range, that is at the mesoscopic scale. The seismic energy attenuation can have a substantial impact on the seismic reflectivity and hence can provide additional information regarding pore fluids saturation (Mavko *et al.* 2005; Dvorkin & Mavko 2006; Quintal *et al.* 2009, 2011; Zhao *et al.* 2014; Mavko *et al.* 2020).

The frequency-dependent amplitude versus offset (FAVO) inversion method is used to estimate seismic velocities and quality factors from pre-stack seismic gathers of partially fluid-saturated reservoirs where higher attenuation of seismic waves is observed. Innanen (2011) carried out a direct AVO inversion process for an-elastic targets from a single absorptive reflectivity event. Teng *et al.* (2012) presented a viscoelastic AVO inversion method by using the Bayesian approach to estimate the seismic wave quality factors and velocities from the imaginary component of pre-stack seismic gathers. Zong *et al.* (2015) proposed an inversion strategy for *P*- and *S*-quality factors from complex seismic data. Chen *et al.* (2018) developed a frequency-dependent AVO approximation and a Markov Chain Monte Carlo (MCMC) inversion to predict inverse seismic quality factors and attenuative seismic impedances. Li & Liu (2019) derived a decoupled viscoelastic AVO equation based on the Aki & Richards (2002) nearly constant Q models which relate the dispersion of *P*- and *S*-wave velocities to the *P*- and *S*-wave quality factors. To avoid decoupling effects in the inversion results due to the simultaneous inversion of multiparameters, they invert only for *P*- and *S*-wave quality factors and density under the assumption of known *P*- and *S*-wave velocities at a dominant frequency in an-elastic medium. However, the inversion process given by Li & Liu (2019) does not take into consideration seismic velocity dispersion effects. Recent advances in frequency-dependent AVO studies and FWI in viscoelastic media include (JafarGandomi & Takenaka 2013; Pang & Stovas 2020; Pan *et al.* 2020; Pan & Wang 2020; Cheng *et al.* 2020; Keating & Innanen 2020; Yang *et al.* 2020; Li *et al.* 2021; Liu *et al.* 2022; Cheng *et al.* 2022); however, the use of the adjoint-state method for non-linear optimization with analytical solutions for the partial derivatives of the gradient of the misfit function for FAVO inversion has not been yet presented.

In this research work, we propose a novel inversion scheme that is a constrained non-linear frequency-dependent AVO algorithm that relies on Li & Liu's (2019) linearized viscoelastic equation. We first develop a generalized seismic forward model for the frequency-angle dependent reflectivity time series by performing a 1-D Fourier transform from frequency-time-angle to frequency–frequency-angle. Then, we apply a gradient descent optimization-based inversion method to iteratively minimize the least-squares misfit function that defines the distance between the forward synthetic model and the observed data. Gradient-based numerical optimization algorithms are highly efficient thanks to the implementation of the adjoint-state method (Plessix 2006) to calculate the gradient. The adjoint-state method is widely used in non-linear inverse geophysical problems (Fabien-Ouellet *et al.* 2017; Wang *et al.* 2021; Guo *et al.* 2022; Yong *et al.* 2022; Ahmed & Weibull 2022; Ahmed *et al.* 2022) and provides the analytical gradient solution more efficiently than the finite difference approximation. For this reason, the adjoint-state method is applied to differentiate the misfit function with respect to the set of viscoelastic AVO variables. We then adopt the chain rule of derivatives to obtain the gradient equations for the *P*- and *S*-wave quality factors. For model updating at every non-linear iteration step, we apply the limited-memory BFGS algorithm (Nocedal & Wright 2006) to define the descent search direction for the data misfit minimization towards the local minima. BFGS is a second-order algorithm for numerical optimization that refers to the class of quasi-Newton methods. L-BFGS performs numerical optimization for large-scale problems very efficiently.

The novelty of the presented inversion process is the analytical derivation of the adjoint-state solution to find the gradient of data misfit with respect to the viscoelastic AVO variables. Furthermore, unlike the Li & Liu (2019) approach, the gradients of seismic (*P*- and *S*-)wave velocities also depend on the frequency and therefore incorporate the velocity dispersion. To validate the FAVO non-linear inversion process, we test the proposed methodology using synthetic data computed from borehole sonic measurements. The direct measurements of seismic wave quality factors during wireline logging is problematic. Therefore, various rock physics models, such as Waters empirical relationships, constant Q models and frequency-dependent White analytical solution (White *et al.* 1975; Waters & Waters 1981; Dvorkin & Mavko 2006; Quintal *et al.* 2009; Li & Liu 2019; Mavko *et al.* 2020), are applied to compute the reference seismic quality factors.

2 THEORY AND METHOD

2.1 Viscoelastic FAVO model

A frequency-dependent reflectivity equation that is a function of seismic velocities, quality factors and density is used to estimate the viscoelastic subsurface properties. In the viscoelastic geological medium, the seismic wave velocity exhibits a dispersion behaviour. Therefore, the reflection coefficients also relate to seismic frequency rather than only incident angles. We implement a forward modelling approach in the frequency domain with the help of a Fourier transform to do convolution in the frequency–frequency-angle domain in order to compute the broadband viscoelastic seismic gather of multilayer dispersive media.

We use the frequency-dependent AVO approximation derived by Li & Liu (2019) for the forward model in the viscoelastic isotropic media. The reflectivity equation in the frequency–time–angle $(\omega^{'}, t, \theta)$ domain is given by:

$$R_{PP}(t,\ \theta,\ \omega_o,\ \omega') = A(\theta)\ \frac{\Delta V_P(t,\ \omega_o)}{V_P(t,\ \omega_o)} + B(t,\ \theta)\ \frac{\Delta V_S(t,\ \omega_o)}{V_S(t,\ \omega_o)} + C(t,\ \theta)\ \frac{\Delta\rho}{\rho} + D(\theta,\ \omega_o,\ \omega')\ \frac{\Delta\xi_P(t)}{\xi_P(t)} + E(t,\ \theta,\ \omega_o,\ \omega')\ \frac{\Delta\xi_S(t)}{\xi_S(t)}, \tag{1}$$

where

$$A = \left[\frac{1}{2}\left(1 + \tan^2\theta\right)\right], \qquad B = \left[-\frac{4\beta^2}{\alpha^2}\ \sin^2\theta\right], \qquad C = \frac{1}{2}\left[1 - \frac{4\beta^2}{\alpha^2}\ \sin^2\theta\right]$$

and

$$D = \left[-\frac{1}{2}(1 + \tan^2\theta)\ \frac{1}{\pi}\ \ln\left(\frac{\omega_o}{\omega'}\right)\right], \qquad E = \left[\frac{4\beta^2}{\alpha^2}\ \sin^2\theta\ \frac{1}{\pi}\ \ln\left(\frac{\omega_o}{\omega'}\right)\right],$$

whereas ω_o refers to the reference angular frequency, while V_P and V_S are the seismic wave phase velocities at an angular reference frequency ω_o and ρ is density. In eq. (1), the denominators represent the average values of elastic and an-elastic properties whereas the Δ-terms are the differences across the viscoelastic geological boundaries. In the forward modelling equation, it is assumed that the medium above and below the interface is viscoelastic and dissipative. The terms ξ_P and ξ_S are defined as functions of both compressional and shear Q-factors, Q_P and Q_S, as:

$$\xi_P(t) = 1 + \frac{1}{Q_P(t)}, \qquad \xi_S(t) = 1 + \frac{1}{Q_S(t)}.$$

Seismic quality factors are not measured directly during borehole logging and are thus computed using empirical equations as in (Waters & Waters 1981; Li 2017) or rock physics models such as Dvorkin–Mavko nearly constant Q approximations (Dvorkin & Mavko 2006; Mavko *et al.* 2020) and the frequency-dependent White's analytical solution (White *et al.* 1975; Quintal *et al.* 2009). The rock physics formulations for the quality factors are given in Appendix A.

2.2 Viscoelastic FAVO inversion

The aim of the FAVO inverse modelling is to retrieve the viscoelastic model properties, that is $m = (V_P, V_S, \rho, Q_P, Q_S)$ based on the broadband seismic data $d(t, \omega^{'}, \theta)$. We first set up the formulation of the seismic FAVO inverse process as the minimization of a differentiable error function J with respect to m using the least-squares error between seismic data (d) and forward model predicted data $f(m)$.

Let j, p and n be the maximum number of reflection interfaces, broad-band frequencies ranges and corresponding incident angles, then the data misfit equation is given by:

$$\min\ J(m) = \min\ \frac{1}{2}\sum_{t=1}^{j}\sum_{\omega'=1}^{p}\sum_{\theta=1}^{n} \parallel d(t,\ \theta) - f(m(t,\ \theta)) \parallel^2 \qquad \text{over} \qquad C, \tag{2}$$

where forward model $f(m)$ is the time-domain convolution after applying the inverse Fourier transform.

$$f(m(t,\ \theta)) = \mathcal{F}^{-1}\sum_{\omega'=1}^{p}\left[W(\hat{\omega}) \cdot R_{PP}(t,\ \theta,\ \hat{\omega},\ \omega')\delta(\omega' - \hat{\omega})\right], \tag{3}$$

whereas, δ represents Dirac's delta function.

In non-linear inverse optimization, an initial guess for the model properties V_P, V_S, ρ, Q_P and Q_S is required to iteratively update the solution, together with a set of constraints to set their physical boundaries:

$$C = \{m = (V_P,\ V_S,\ \rho,\ Q_P,\ Q_S)\ \mid\ m_{\min}\ \leq\ m\ \leq\ m_{\max}\}. \tag{4}$$

The gradient of the data misfit J described in eq. (2) is the vector of partial derivatives of the misfit error J in respect of model properties m as given:

$$\nabla J = \left[\frac{\partial J}{\partial V_P},\ \frac{\partial J}{\partial V_S},\ \frac{\partial J}{\partial \rho}\ \frac{\partial J}{\partial Q_P},\ \frac{\partial J}{\partial Q_S}\right] \tag{5}$$

and the solution of misfit J with respect to $m = [V_P, V_S, \rho, Q_P, Q_S]$ is

$$\frac{\partial J}{\partial m} = -\Big[d - f(V_P,\ V_S,\ \rho,\ Q_P,\ Q_S)\Big] \cdot \frac{\partial f}{\partial m}. \tag{6}$$

In practical applications, viscoelastic seismic properties are discretized at the interfaces $i = 1, \ldots\ i_n$ in the time (or depth) domain. Therefore, in the following, we adopt the discretized notation for all the model variables

$$m = [V_{P1},\ \ldots,\ V_{Pi_n},\ V_{S1},\ \ldots,\ V_{Si_n},\ \rho_1,\ \ldots,\ \rho_{i_n},\ Q_{P1},\ \ldots,\ Q_{Pi_n},\ Q_{S1},\ \ldots,\ Q_{Si_n}]^T.$$

2.3 Adjoint-state method and L-BFGS

The adjoint-state method provides an effective numerical approach to computing the gradient of the non-linear least-square data misfit that relies on a set of state variables without computation of the Fréchet derivatives. The adjoint solution is implemented here by introducing the augmented Lagrangian function $\mathcal{L}$ as:

$$\mathcal{L}(V_P,\ V_S,\ \rho,\ \xi_P,\ \xi_S,\ R_{PP},\ \lambda) = \sum_i \int_\theta \mathrm{d}\theta \Big[d[i] - f[i]\Big]^2 + \sum_i \int_{\theta,\,\omega} \mathrm{d}\theta \left[R_{PP}[i] - A[i]\ \frac{\Delta\alpha}{\alpha} - B[i]\ \frac{\Delta\beta}{\beta} - C[i]\ \frac{\Delta\rho_0}{\rho_0} - D[i]\ \frac{\Delta\Xi_P}{\Xi_P} - E[i]\ \frac{\Delta\Xi_S}{\Xi_S}\right] \lambda_{[i]}, \quad (7)$$

where λ refers the adjoint-state variable, R_{PP} denotes the state variable and forward model f is given by the eq. (3). The Lagrangian function in eq. (7) can be reformulated as $\mathcal{L} = J(R_{PP},\ m) + C(R_{PP},\ m) * \lambda$, where the constraint ($C$) in the Lagrangian formalism is automatically satisfied by:

$$\left[R_{PP}[i] - A[i]\ \frac{\Delta\alpha}{\alpha} - B[i]\ \frac{\Delta\beta}{\beta} - C[i]\ \frac{\Delta\rho_0}{\rho_0} - D[i]\ \frac{\Delta\Xi_P}{\Xi_P} - E[i]\ \frac{\Delta\Xi_S}{\Xi_S}\right] = 0. \quad (8)$$

In eq. (7), the denominators indicate the average values at the interfaces and the numerators are the differential values across the interfaces. To make the derivation of the gradient solution of the Lagrangian of the misfit function ease for ourselves, we replace the seismic velocities, density and quality factor terms in eq. (7) with α, β, ρ_0, Ξ_P and Ξ_S which are related to the model variables m as:

$$\alpha[i] = \frac{V_P[i+1] + V_P[i]}{2} \qquad \Delta\alpha[i] = V_P[i+1] - V_P[i]$$

$$\beta[i] = \frac{V_S[i+1] + V_S[i]}{2} \qquad \Delta\beta[i] = V_S[i+1] - V_S[i]$$

$$\rho_0[i] = \frac{\rho[i+1] + \rho[i]}{2} \qquad \Delta\rho_0[i] = \rho[i+1] - \rho[i]$$

$$\Xi_S[i] = \frac{\xi_S[i+1] + \xi_S[i]}{2} \qquad \Delta\Xi_S[i] = \xi_S[i+1] - \xi_S[i]$$

$$\Xi_P[i] = \frac{\xi_P[i+1] + \xi_P[i]}{2} \qquad \Delta\Xi_P[i] = \xi_P[i+1] - \xi_P[i].$$

The gradient solution of the data misfit is achieved by solving the subsequent adjoint-state equations:

$$\frac{\partial\mathcal{L}}{\partial R_{PP}} = 0, \qquad \frac{\partial\mathcal{L}}{\partial\lambda} = 0. \quad (9)$$

The analytical formulation of the partial derivatives is given in Appendix B.

When the adjoint eqs (9), the partial differentials of the Lagrangian function in respect of viscoelastic R_{PP} and state variable λ are satisfied, that is equal to 0. Then the partial derivatives coincide with:

$$\frac{\partial\mathcal{L}}{\partial\cdot} = \frac{\partial J}{\partial\cdot},$$

where $\cdot$ represents one of the five unknown variables m. Then the partial derivatives with respect to P- and S-quality factors are acquired using the chain rule derivative:

$$\frac{\partial J}{\partial Q_P[i]} = \frac{\partial J}{\partial\xi_P[i]} \cdot \frac{\partial\xi_P[i]}{\partial Q_P[i]} \quad (10)$$

$$\frac{\partial J}{\partial Q_S[i]} = \frac{\partial J}{\partial\xi_S[i]} \cdot \frac{\partial\xi_S[i]}{\partial Q_S[i]} \quad (11)$$

$$\frac{\partial\xi[i]}{\partial Q_P[i]} = -\frac{1}{Q_P^2[i]}, \qquad \frac{\partial\xi_S[i]}{\partial Q_S[i]} = -\frac{1}{Q_S^2[i]}. \quad (12)$$

The model m, including the five unknown variables, is updated at every iteration using the second-order quasi-Newton L-BFGS optimization technique that iteratively approximates the inverse Hessian ($H^{(k)}$) based on the gradient values and the previous solution as:

$$m^{(k+1)} = m^{(k)} + \alpha^{(k)}[-H^{(k)}\nabla J], \quad (13)$$

whereas $m^{(k)}$ and $m^{(k+1)}$ are referred as the current and updated values and $\alpha^{(k)}$ is described as step length. The gradient descent search direction is determined by $[-H^{(k)}\nabla J]$. The L-BFGS procedure is described in algorithm 1.

The physics involving seismic wave velocities and corresponding seismic quality factors are coupled in the simultaneous viscoelastic inversion (Kamei & Pratt 2013). Consequently, the inverse solution of the estimation of the parameters in presence of low-resolution noisy data is not unique and the prediction of velocities and quality factors might be inaccurate. The lack of model properties resolution is referred to as crosstalk or trade-off between the variables. Operto *et al.* (2013) present different strategies to reduce the coupling effect between

Algorithm 1 The standard L-BFGS algorithm

1: **L-BFGS procedure**
2: Choose a stating value $\mathbf{m}_0$, and integer $l > 0$
3: do $k = 0, 1, 2, 3 \ldots$
4: Calculate data misfit value J and gradient ∇
5: Compute the search direction $[-\mathbf{H}^{(k)} \nabla J]$ using L-BGFS two-loop recursion
6: Find the step length $\alpha^{(k)}$ using line search algorithm
7: First trial step length: $\alpha^{(0)} = l/\|\nabla^0\|^2$, if $k >$ **m** try $\alpha^{(k,0)} = 1$
8: do $i = 0, 1, 2, 3 \ldots, l$
9: Verify function minimization conditions
10: Get new $\alpha^{(k,i+1)}$ using line search algorithm
11: End do
12: Update $\mathbf{m}^{(k+1)} = \mathbf{m}^{(k)} + \alpha^{(k)}[-\mathbf{H}^{(k)} \nabla J]$
13: Repeat until convergence
14: **End procedure**

optimized properties, such as the use of second order Hessian matrix, the selection of an appropriate parametrization and a model-driven approach where the more sensitive variables are estimated before the least sensitive ones.

The linearized AVO equation for viscoelastic media relies on a set of five variables, that is *P*- and *S*-wave velocities, density, and the seismic quality factors (V_P, V_S, ρ, Q_P, Q_S). In this model, the crosstalk affects the following couples of variables: V_P and Q_P, V_S and Q_S, V_P and V_S and Q_P and Q_S. To examine the crosstalk effects between model variables, we run several tests and study the coupling effects between seismic velocities and quality factors at initial iterations as well as for low and high incident angles. In the first crosstalk test, we introduced two perturbations for *P*- and *S*-wave velocities (e.g. $\Delta V = 50$ and 200 ms^{-1}) and computed the gradient of corresponding quality factors. In theory, if the velocities and quality factors were independent, the perturbation in V_P or V_S with a constant corresponding Q_P and Q_S, respectively should not affect the partial derivatives with respect to the quality factors. However, in reality, these parameters are not independent and the partial derivatives of the quality factors are affected by the velocity perturbation. Fig. 1(a) shows the results of the perturbation for the following couples: V_P and Q_P, V_S and Q_S, by comparing the gradient results with and without perturbation. The results demonstrate that strong crosstalk exists between the variables, as a small perturbation in the seismic velocities results in a variation in the corresponding quality factors. We also investigate the crosstalk between V_P and V_S as well as Q_P and Q_S derived through a rock physics model by considering the WIFF mechanism. The perturbations are added to the compressional wave velocity and the related quality factor. The gradients of V_S and Q_S with and without perturbations are shown in Fig. 1(b). The gradients plotted in Fig. 1 are scaled by different factors ranging between 10^3 and 10^5. The results show limited crosstalk between V_P and V_S and quality factors. Despite the large perturbation in the *P*-wave quality factor, limited crosstalk between Q_P and Q_S is observed. Then, we study the crosstalk effects between two classes (V_P and Q_P, and V_S and Q_S) at low and high incident angles (Fig. 2). The results show that the crosstalk between variables exists at different incident angles: for example, at the near offset, the coupling between V_P and Q_P is higher than the coupling between V_S and Q_S for large offset; this result is even more evident for the coupling between V_S and Q_S.

Due to the coupling between seismic velocities and corresponding quality factors, we adopt the strategy of inverting the most sensitive model variables first (V_P, V_S and density) and then predicting the least sensitive properties (Q_P and Q_S). The crosstalk between V_P and V_S or Q_P and Q_S is limited; hence, it does not affect the inversion of seismic velocities at the first phase nor the inversion of the quality factors in the next step.

3 APPLICATIONS

We present several applications with two synthetic data sets to verify the described FAVO inversion scheme by using the frequency-domain convolution of broadband signals. Data set 1 represents a 1-D vertical profile, whereas data set 2 represents a 2-D seismic section. In both examples, the quality factors have been computed from well logs using empirical and rock physics models (Appendix A).

In the first example, a 1-D synthetic seismic forward model obtained from wireline logs in the Edvard Grieg field located in the North Sea is used. The quality factors are calculated using the empirical expressions given by eq. (A1). The reference model is upscaled at the seismic scale (Fig. 3). The seismic response with signal-to-noise ratio infinity and with seismic random noise level (S/N = 50) is shown in Fig. 4. Seismic reflection amplitudes are displayed up to the incident angle 30° with an interval of 5°. Figs 4 and 5 present the results of the inversion scheme for the elastic and an-elastic properties. In the case of S/N = 0, the inversion method shows good convergence, and the estimated parameters are in close agreement with the reference properties (Fig. 5). In the case of noisy data, the inversion method produces stable results for *P*- and *S*-wave seismic velocities and density are consistent with the reference models, whereas the inversion of quality factors are more unstable and less accurate (Fig. 6). To reduce the instability of the solution, we apply small Tikhonov regularization weights (Aster *et al.* 2018), whereas the inaccuracy is due to noise in the seismic data and the limited sensitivity of the forward model.

In example 2, we applied the proposed non-linear inversion process on a 2-D synthetic example mimicking faulted geological boundaries and inclined horizons. Seismic velocities interpreted in seismic velocity analysis during processing are used to generate a 2-D visco-elastic

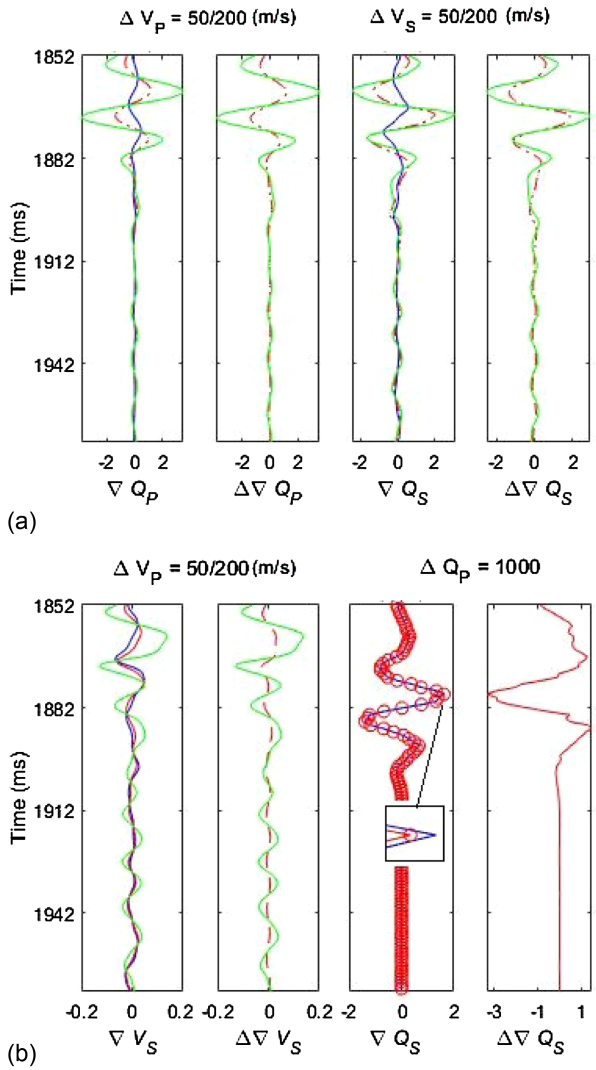

Figure 1. Crosstalk between elastic and an-elastic variables; V_P and Q_P, V_S and Q_S and Q_P and Q_S (a), and V_P and V_S and Q_P and Q_S (b). The panels represent the gradients: red lines indicate a perturbation of 50 m s^{-1}, green lines indicate a perturbation of 200 m s^{-1}, and blue lines indicate no perturbation. The crosstalk between Q_P and Q_S is calculated based on the rock physics model.

model. The FAVO inversion process is implemented trace by trace in the entire time window (0–5000 ms). The resulting elastic and viscoelastic properties are shown in Fig. 7. The inverted *P*- and *S*-wave velocity, density and the related seismic quality factors are accurately estimated. The initial *Q*-factors are obtained by using the empirical expressions. The inversion produces some mismatches, especially in the density prediction, which can be partially compensated using Tikhonov regularization.

In the next examples, we focus on partially saturated reservoirs to investigate frequency-dependent mechanisms. A leading cause of seismic wave attenuation and velocity dispersion in partially fluid-saturated rock or sediments is WIFF. Fig. 8 shows the P wave attenuation behaviour in two cases when the magnitude of attenuation is estimated as frequency independent (constant *Q* model, Fig. 8a) and frequency-dependent (Figs 8b and c) in a partially saturated rock. Partially saturated gas reservoirs exhibit higher attenuation compared to oil and water. Furthermore, partially saturated reservoirs exhibit the *P*-wave energy dissipation which also varies as a function of seismic frequencies. In the next examples, we adopt a rock physics model for seismic (*P*- and *S*-) wave attenuation due to WIFF in an oil–water system.

In example 3, we first adopt a simple physically based model with constant *Q* (eqs A2–A5) which allows for estimating the *P*- and *S*-wave attenuation from the well logging curves. This model provides reasonable attenuation curves without considering frequency-dependence effects and can be easily incorporated into the seismic model (Dvorkin & Mavko 2006). The model example in Fig. 9 is taken from the Edvard Grieg oil field located in the North Sea. The reservoir zone (1865–1888 ms) has a partial oil saturation of about 66 per cent. Fig. 9 shows the water saturation curve and the computed attenuation curves in the corresponding zones. The calculated *P*-wave attenuation due to WIFF is shown in Fig. 9(b). The partially oil-saturated zone displays higher attenuation due to partially fluid saturation heterogeneities, for example the seismic energy loss in the oscillatory pore-fluid flow induced by the passage of waves. The seismic wave passage induces fluid pressure gradients which cause the fluid flow between softer-stiffer fluids patches, which then results in viscus-friction losses. The Q_P^{-1} is approximately zero in the water zone as low and high limit moduli become equal. Fig. 9(c) shows both the theoretical *P*- and *S*-wave

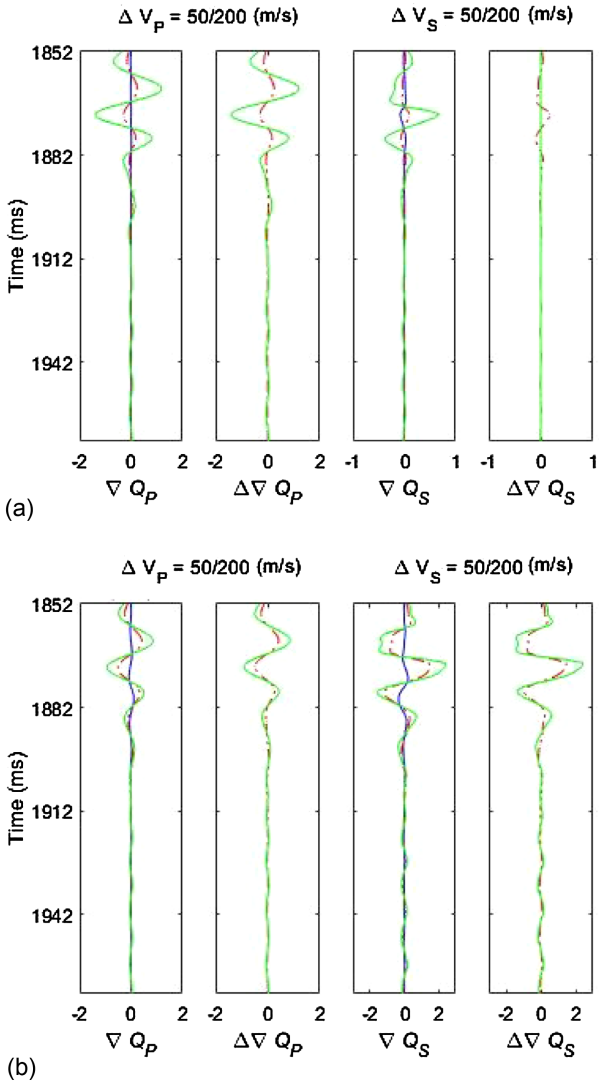

Figure 2. Crosstalk between elastic and an-elastic variables; V_P and Q_P, V_S and Q_S, at incident angles of 1−5° (a) and at incident angles of 25−30° (b). The panels represent the gradients: red lines indicate a perturbation of 50 m s^{-1}, green lines indicate a perturbation of 200 m s^{-1}, and blue lines indicate no perturbation.

attenuation curves for fully water-saturated rocks, where the attenuation depends on the heterogeneities of both fluid and the solid phase. The *P*-wave attenuation shown in Fig. 9(d) accounts for attenuation due to partial fluid saturation, full water saturation, and solid frame heterogeneities. The quality factors (Q_P and Q_S) are shown in Fig. 10. The properties used in the rock physics model are given in Table 1.

We then apply the inversion method to estimate the energy dissipation from the seismic frequency-angle gather. The seismic response up to 30° with intervals of 5° (Fig. 10a) together with initial guesses and true models for Q_P and Q_S are shown in Fig. 10(b). The inversion results are shown in Fig. 10(c): the *P*-wave quality is accurate whereas there is a mismatch between the *S*-wave quality factor predictions, possibly because of the low sensitivity of the seismic data to the shear wave attenuation due to rock-fluid inhomogeneities.

In example 4, we test the inversion workflow for the frequency-dependent mesoscopic loss which is responsible for the *P*- wave seismic energy dissipation mechanisms at seismic frequencies range (Tisato & Quintal 2013). The magnitude of the seismic energy attenuation is associated with both characteristics of the reservoir strata and of the fluid within pores (Carcione & Picotti 2006). We model the frequency-dependent Q_P based on White's analytical solution (Appendix A) at various vertical locations by using the well log data with the parameters given in Table 1. We then apply the inversion technique to invert the seismic frequency-dependent *P*-wave quality factors. The results for a subset of frequencies are shown in Fig. 11 in the partially saturated reservoir zone. The inverted Q_P curves are in good agreement with the reference models, especially at lower frequencies. Fig. 12 shows a comparison of the theoretical *P*-wave attenuation computed from White's model and the predicted *P*-wave attenuation estimated with the inversion method, which has been made for a broad range of seismic frequencies and demonstrates a high good correlation. This shows the efficiency of the inversion process to estimate the fluids-related attenuation from seismic gather. Thus, our proposed inversion method can be used to locate partially hydrocarbon zones. At higher frequencies, the FAVO inversion overestimates the *P*-wave attenuation but the difference in magnitude is small.

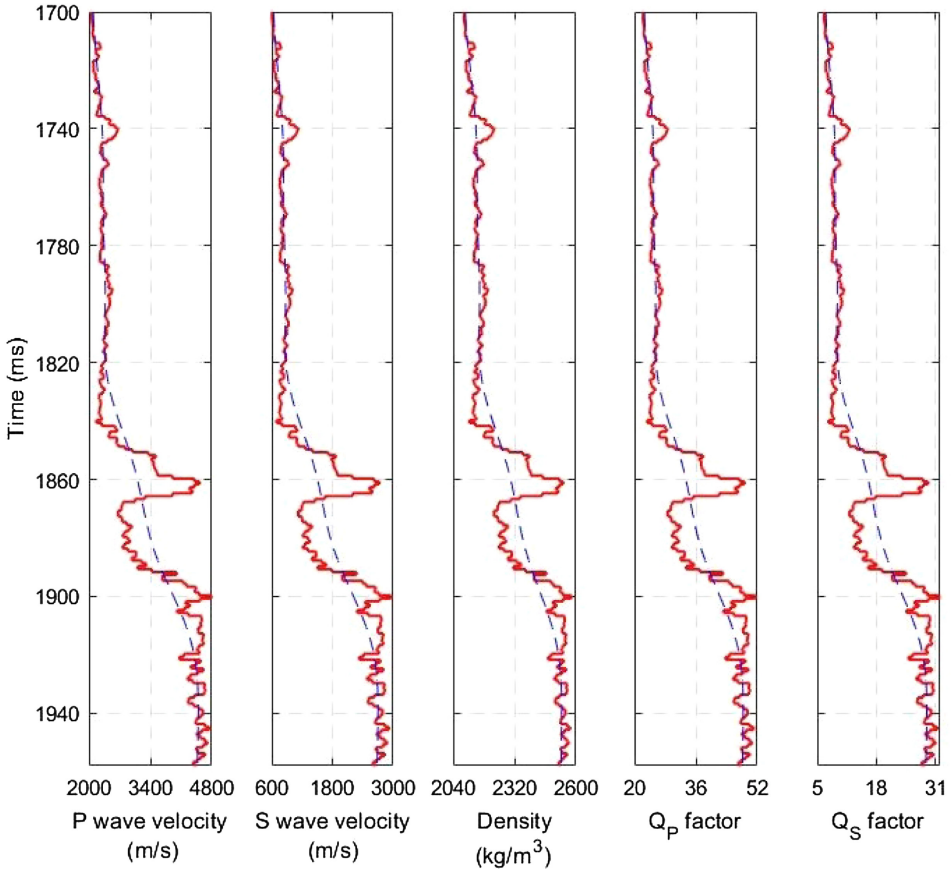

Figure 3. Example 1—Reference model variables including *P*- and *S*-wave velocities, density and *P*- and *S*-quality factors, with respective initial guesses.

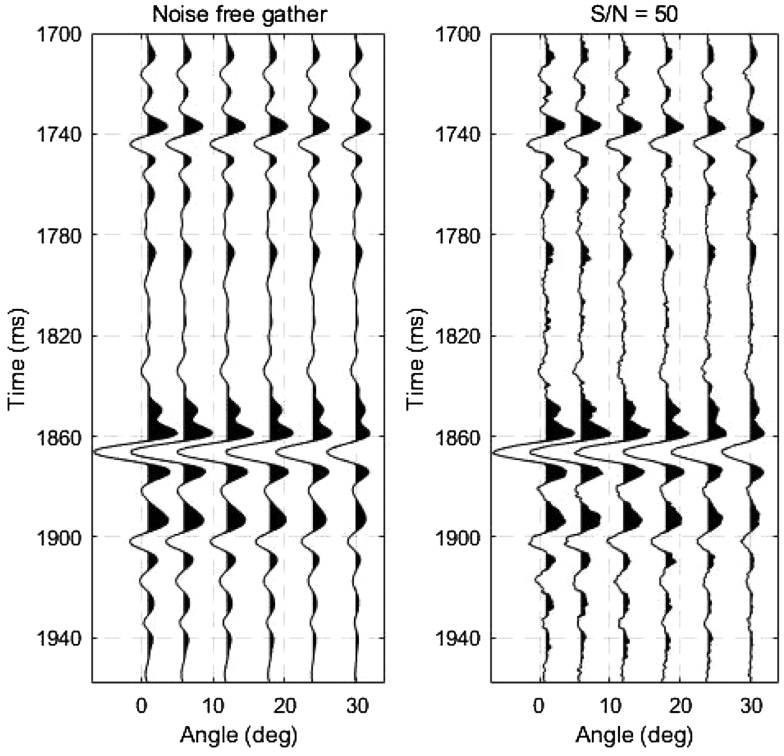

Figure 4. Example 1—Synthetic seismic pre-stack gathers with different noise levels (no noise and S/N = 50).

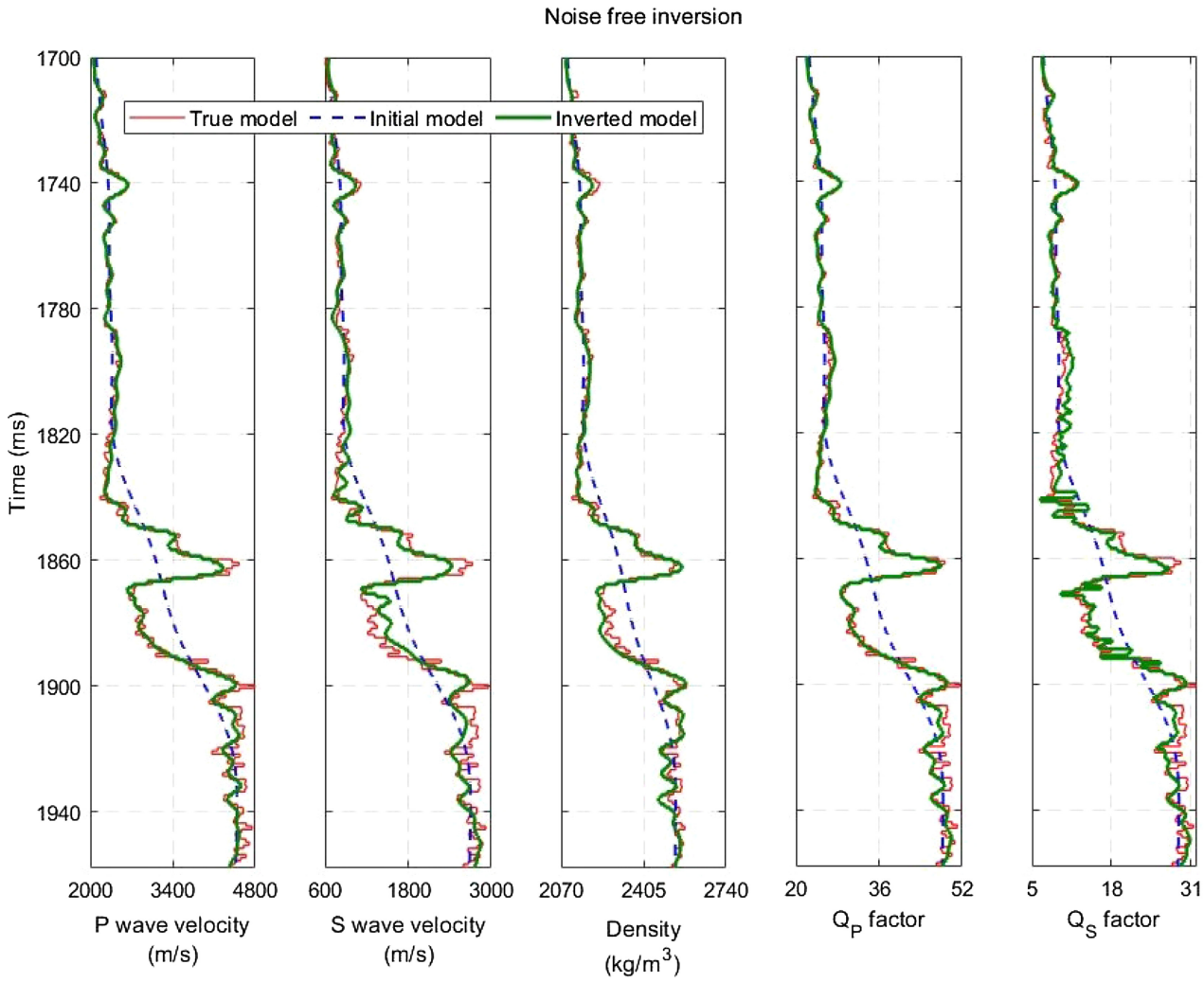

Figure 5. Example 1—Inverted model variables including *P*- and *S*-wave velocities, density and *P*- and *S*-quality factors.

Finally, we propose an uncertainty quantification study where we investigate the uncertainty of the solution as a function of the variability of the initial model. The uncertainty is quantified using a Monte Carlo simulation where we generate a set of initial models and predict the corresponding set of posterior solutions. The variability of the posterior ensemble of solutions is used to investigate the uncertainty propagation with respect to the initial uncertainty. We first generate a set of 75 initial models of the five unknown model variables by sampling from a multivariate Gaussian distribution estimated from the well logs of the properties. The initial models are simulated according to a spatial correlation model (Grana *et al.* 2021) estimated from the well log (Fig. 13). We then apply the proposed inversion method to each initial realization to obtain the distribution of the inverted models (Fig. 14). The uncertainty in the inverted models of the model variables is relatively narrow despite the large variability in the initial realizations, which shows that the presented inversion scheme is very stable and precise.

4 DISCUSSION

The proposed inversion is relying on the gradient descent method which requires the computation of the first-order gradients of the data misfit in respect of the unknown model variables. By defining the Lagrangian formulation, we derive the adjoint solutions and the gradients of the data misfit function, leading to a more efficient algorithm compared to the classic non-linear inverse theory. Furthermore, the optimal solution is obtained by minimizing the misfit function iteratively and by using the non-linear L-BFGS optimization method.

Global optimization is often used in seismic inverse modelling (Sen & Stoffa 2013) thanks to its ability to explore the model space and avoid local minima; however, for the proposed seismic inverse problem, local optimization can produce results comparable to global optimization with a lower computational cost, as seismic data provide relative information about the property contrasts at the interfaces and the solution is expressed as a perturbation of the low-frequency model. Because of the seismic noise and the band-limited nature of the

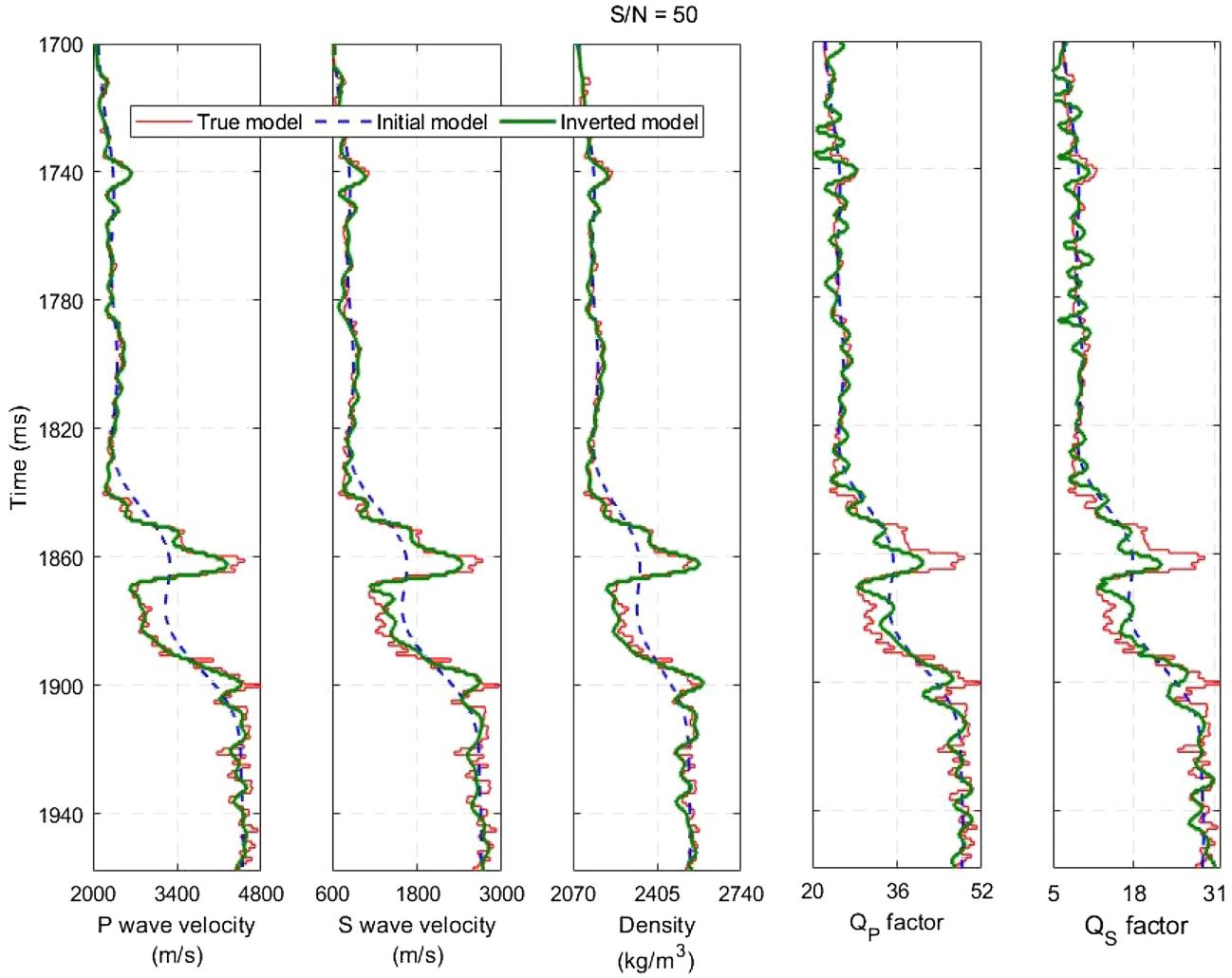

Figure 6. Example 1—Comparison of initial and inverted properties estimated from the noisy seismic data.

seismic data, the solution is not unique and the objective function might include several local minima. For this reason, we propose a sensitivity study on the initial guess of the inversion to investigate the variability of the solution with respect to the initial model. On the other hand, the Bayesian methods for seismic inverse problems (Mosegaard & Tarantola 1995; Sen & Stoffa 1996; Buland & Omre 2003; Doyen 2007; Avseth *et al.* 2010; Grana *et al.* 2021) can be extended to viscoelastic inversion; however, the computational efficiency of the Bayesian inverse methods generally requires assumptions on the linearization of the forward model and the Gaussian distribution of the model variables. In the Bayesian context, Monte Carlo simulation methods can also be applied for non-linear inverse problems with complex prior models (Cordua *et al.* 2012; de Figueiredo *et al.* 2019), but the application to large geophysical data sets is generally not feasible because of the spatial correlation of the model variables (Grana *et al.* 2022).

The forward model is relying on the frequency-angle dependent linearized AVO equation derived from constant Q models for the P- and S-wave quality factors, where the seismic response depends on the incident angles and the seismic frequencies. In the objective function of the inversion, we did not apply weights associated with angles nor frequencies, as the calibration of such weights is often challenging as it depends on uncertain information such as acquisition and processing parameters. In the inversion, all frequencies and angles are used simultaneously to define the update direction of the optimization step. Hierarchical approaches for the sequential inversion with respect to the frequency or angles could also be applied but it might strengthen the crosstalk. The proposed inversion accounts for the velocity dispersion in both P- and S-wave velocities as the derived gradient eqs (B1) and (B2) for V_P and V_S variables are frequency-dependent. The inversion predicts the model variables by simultaneously modelling the multi-angles broad-band frequencies.

The viscoelastic inversion shows crosstalks between model variables, specifically seismic velocities and quality factors. Based on our tests, the velocity variables are dominant over the quality factors; hence to avoid the crosstalk, we perform the inversion in two steps: first, we invert the seismic data for the most sensitive properties, for example seismic velocities and bulk density; then we apply inversion process for the less sensitive variables, for example quality factors. This approach provides stable inversion results for less sensitive properties. In

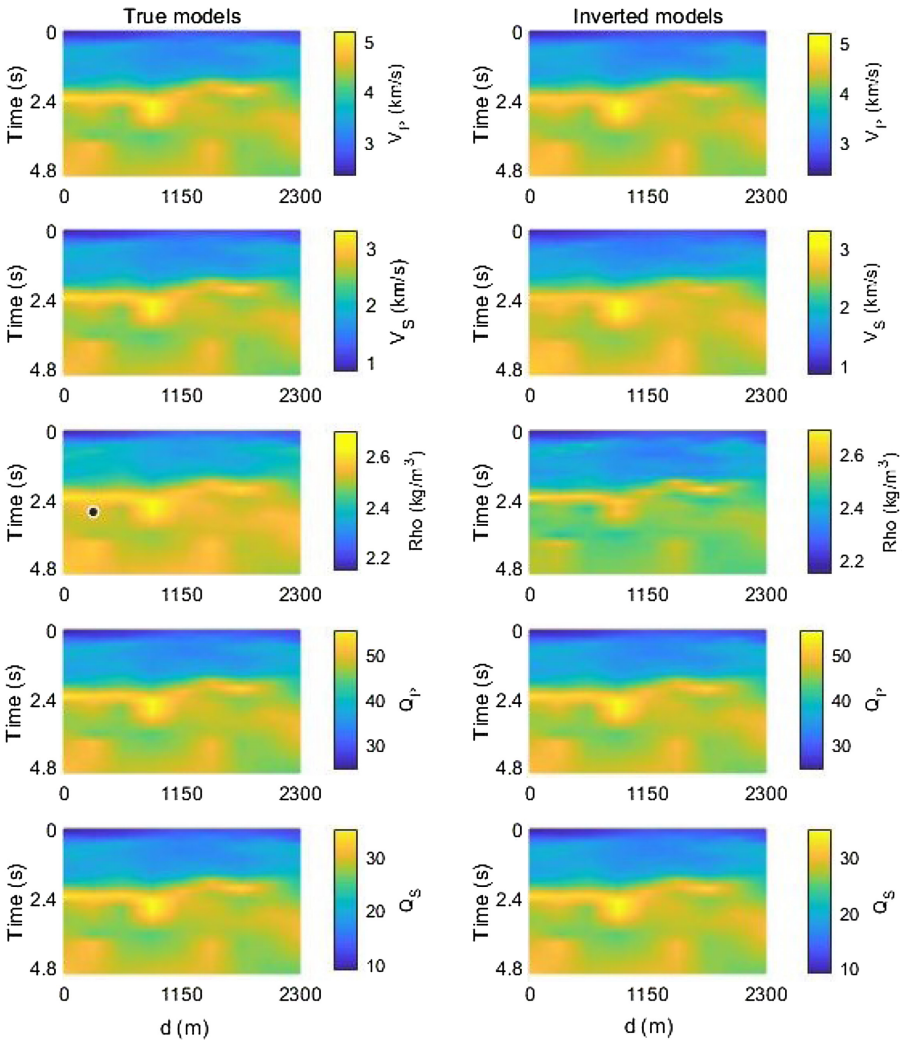

Figure 7. Example 2—Reference model variables (left-hand panel) and inverted variables (right-hand panel) including *P*- and *S*-wave velocities, density and *P*- and *S*-quality factors.

general, due to a lower sensitivity of the shear wave quality factor to the seismic data, it is more challenging to accurately estimate the Q_S when the seismic data is noise contaminated.

The proposed sensitivity analysis aims to quantify the uncertainty of the inverted model as a function of the variability of the initial models. Approximate Bayesian Computation and Markov chain Monte Carlo methods could also be used to assess the posterior uncertainty in a Bayesian setting; however, the computational cost of these techniques is generally higher than the proposed sensitivity. Another approach for uncertainty quantification in the context of local optimization is the calculation of the inverse Hessian matrix around the convergence point as a proxy to the model covariance matrix, which provides an estimate of the null space around the solution of the optimization problem.

One of the main limitations of the described method is the instability of the solution for the quality factors in case of noisy data. This effect can be mitigated by Tikhonov regularization which improves the stability of the optimized model. The solution shows some dependency on the initial model possibly due to the presence of noise in the data, the approximation of the seismic forward model, and the local minima of the objective functions; however, the proposed uncertainty quantification captures the variability of the solution as a function of the uncertainty of the initial model.

5 CONCLUSIONS

We proposed a constrained non-linear frequency-angle-dependent pre-stack inversion method to estimate seismic properties in viscoelastic media. The inversion of an-elastic properties, which are the *P*- and *S*-wave attenuation described as inverse quality factors (Q_P and Q_S), in addition to seismic velocities and density, provides high-resolution seismic images which can be used in the geophysical exploration and seismic monitoring of hydrocarbon fields, as well as in geothermal energy or geological sequestration of CO_2. The inversion algorithm relies

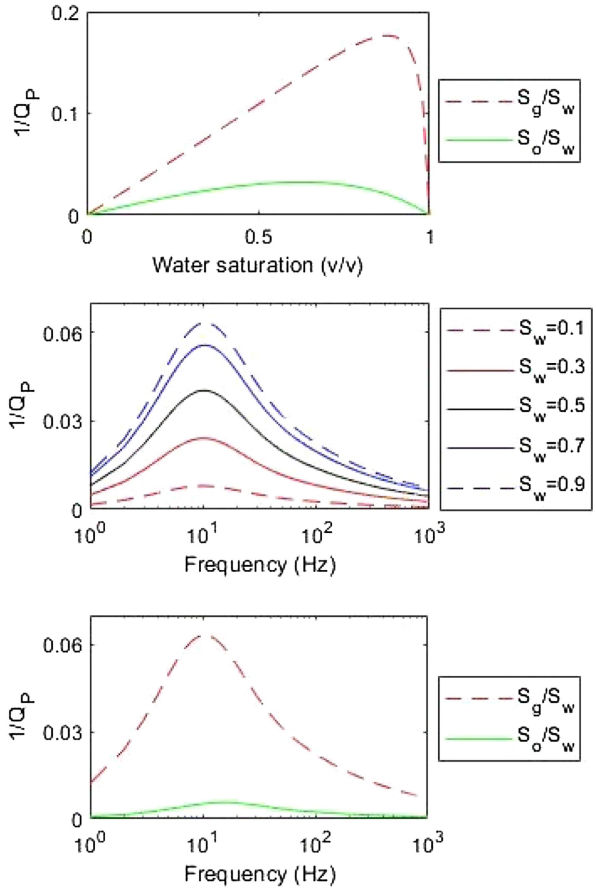

Figure 8. *P*-wave attenuation results: (top panel) *P*-attenuation as a function of water saturation estimated by using nearly constant *Q*-model (red dashed line for the gas–water case and solid green line for the oil–water case); (middle panel) *P*-attenuation as a function of frequencies at different gas–water saturation computed at mesoscopic scale using White's analytical solution and (bottom panel) *P*-attenuation for the gas–water and oil–water cases as a function of frequency in the case of $S_w = 0.9$ at the mesoscopic scale.

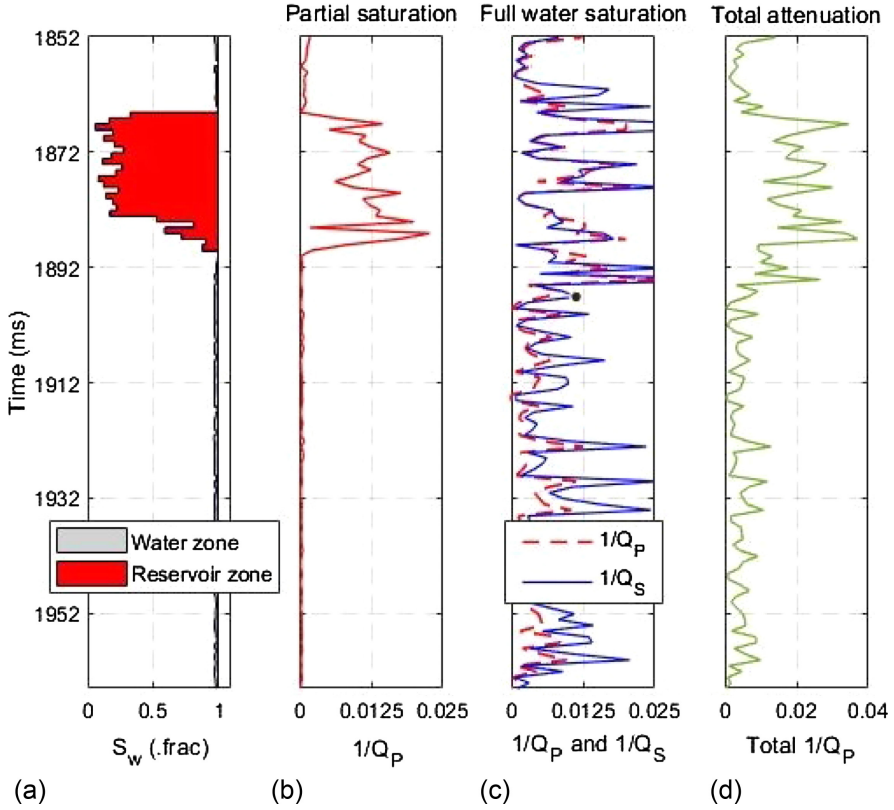

Figure 9. Example 3—Water saturation (a) and corresponding *P*-wave attenuation (b–d): (b) attenuation due to pore fluid heterogeneities in partially saturated rocks; (c) attenuation due to pore fluid heterogeneities in fully water-saturated rocks and (d) the total attenuation due to both fluid and solid frame heterogeneities.

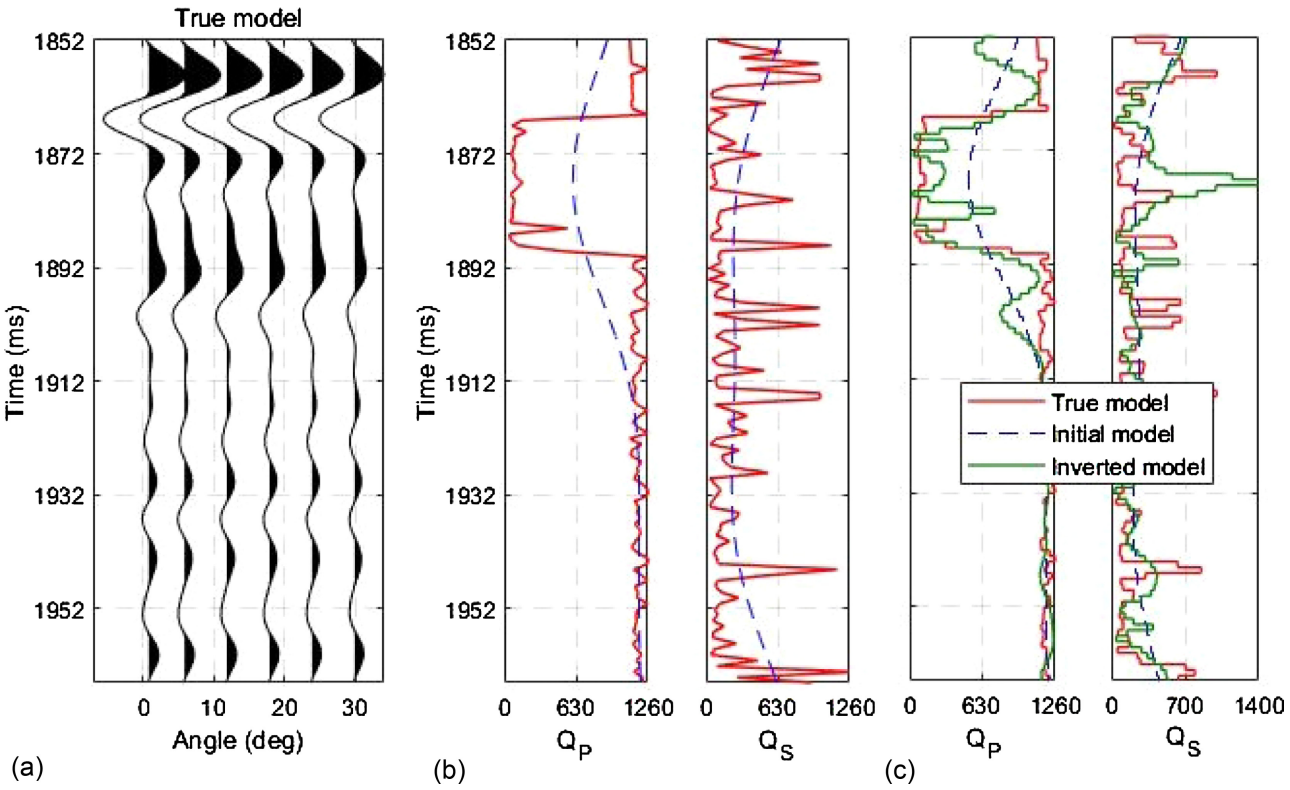

Figure 10. Example 3—Seismic response up to the incident angle 30° (a), *P*- and *S*-wave quality factors calculated from the attenuation logs are given in the Fig. 9 (b), and the inverted *P*- and *S*-wave quality factors estimated by using constant *Q* rock physics models (c). The solid red curves are the reference models and the dashed blue curves represent the initial models.

Table 1. The reservoir rock and fluid parameters used in rock physics models, based on lab measurements and literature values (Mavko *et al.* 2020).

Parameters	Average values
Effective porosity (ϕ)	0.26
Permeability (k)	50 mD
Bulk modulus of quartz	37 (GPa)
Bulk modulus of clay	21 (GPa)
Shear modulus of quartz	44 (GPa)
Shear modulus of clay	7 (GPa)
Layer 1 thickness (d_1)	0.20 (m)
Layer 2 thickness (d_2)	0.50 (m)
Temperature (T)	78.18 (°C)
Pressure (P_e)	26 (MPa)
Oil API	35
Gas–oil ratio (GOR)	145.7
Density of water (ρ_o)	987 (kg m^{-3})
Density of oil (ρ_o)	821 (kg m^{-3})
Bulk modulus of oil (K_o)	1.04 (GPa)
Bulk modulus of water (K_o)	2.55 (GPa)
Water viscosity (η_w)	0.001 (Pa.s)
Oil viscosity (η_o)	0.11 (Pa.s)

Table 2. Symbols used for the elastic moduli given in the eqs (A12)–(A14).

Symbol	Parameter
E_G	Plane *P*-wave modulus of saturated rock
K_E	Effective bulk modulus
r	Ratio of fast *P*-wave fluid tension to total normal stress ratio
K_{sat}	Gassmann modulus
E_d	Dry-rock fast *P*-wave modulus
M	Solid-grain bulk modulus
β_c	Biot's coefficient
K_d	Frame bulk modulus
K_m	Solid bulk modulus
μ_d	Shear modulus

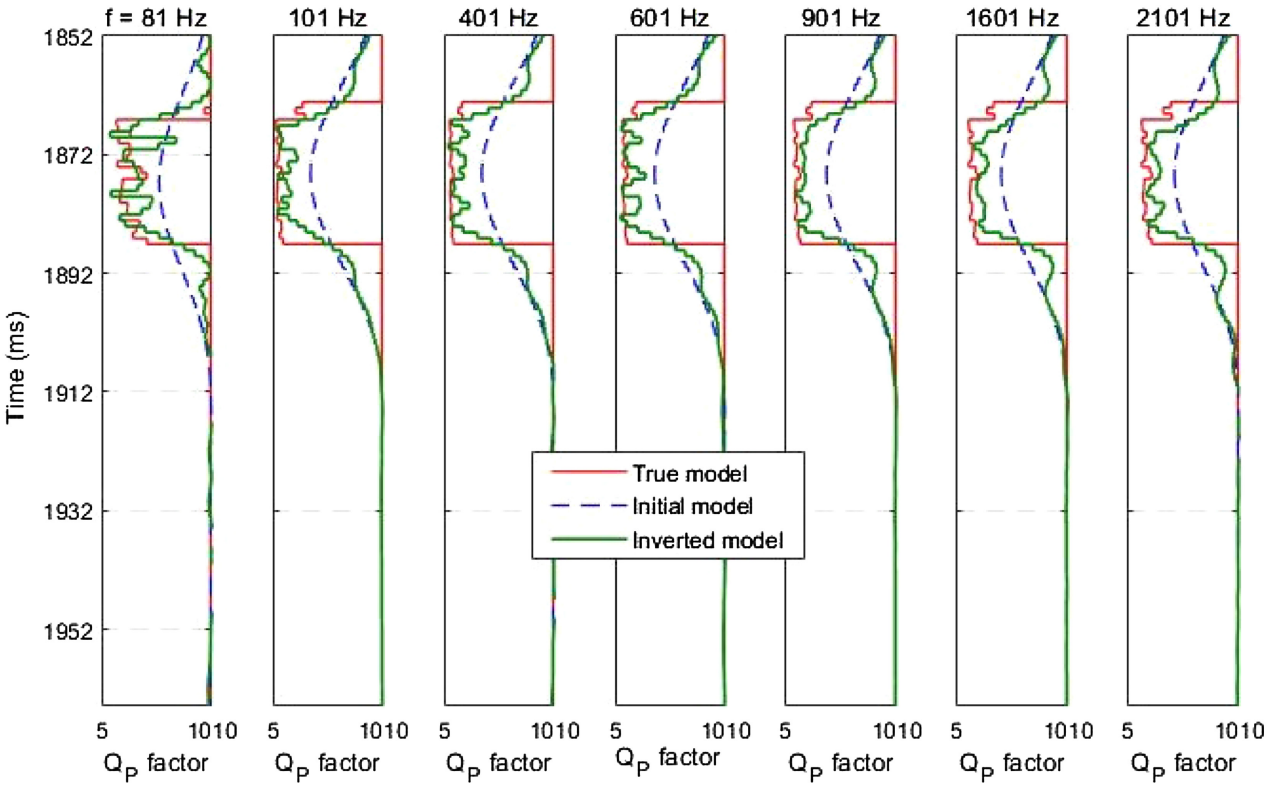

Figure 11. Example 4—Inverted Q_P at different frequencies together with reference and initial models. The inversion results show a good correlation with the true models.

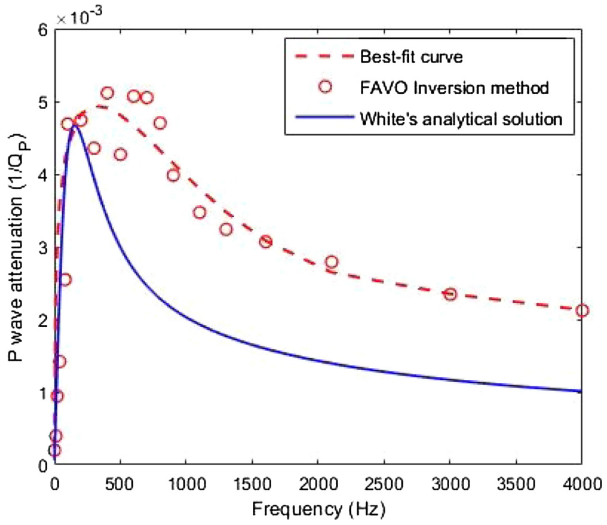

Figure 12. Example 4—Comparison of *P*-wave attenuation curves computed using approximated White's analytical solution (blue curve) and the proposed FAVO inversion method (red curve).

on the gradient descent optimization technique in which a differentiable misfit function is iteratively minimized by using a second-order non-linear L-BFGS algorithm. The least-square misfit function is based on an angle-frequency-dependent forward model of broadband signals in the frequency domain. The first-order derivatives of the misfit function in respect of five model variables are analytically obtained using the adjoint-state technique and chain rule of derivatives, which results in an accurate and efficient implementation. The inversion method was tested on synthetic examples, in 1-D and 2-D, to predict the quality factors and validated for different an-elastic mechanisms and noise-contaminated seismic data. The results demonstrate that the proposed an-elastic non-linear AVO inversion process accurately retrieves

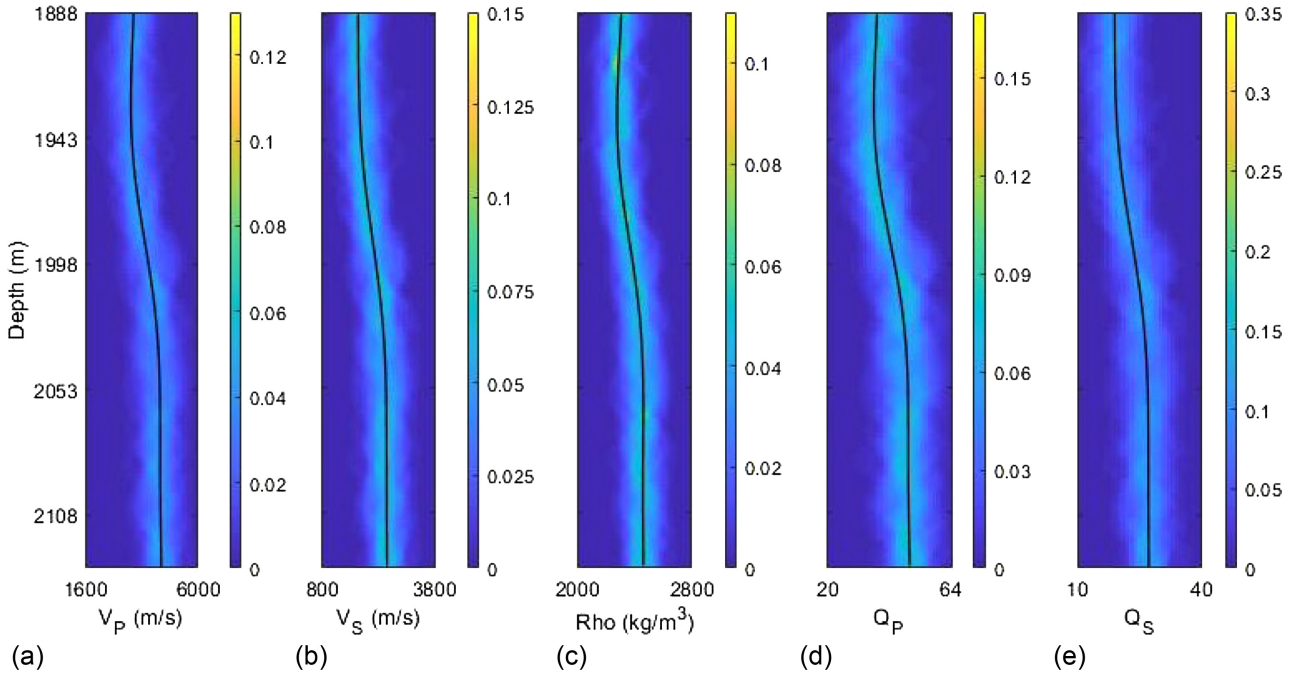

Figure 13. Initial realizations of *P*-wave velocity (a), *S*-wave velocity (b), density (c), *P* (d) and *S* (e) wave quality factors. The mean of the initial models is also shown in black colour.

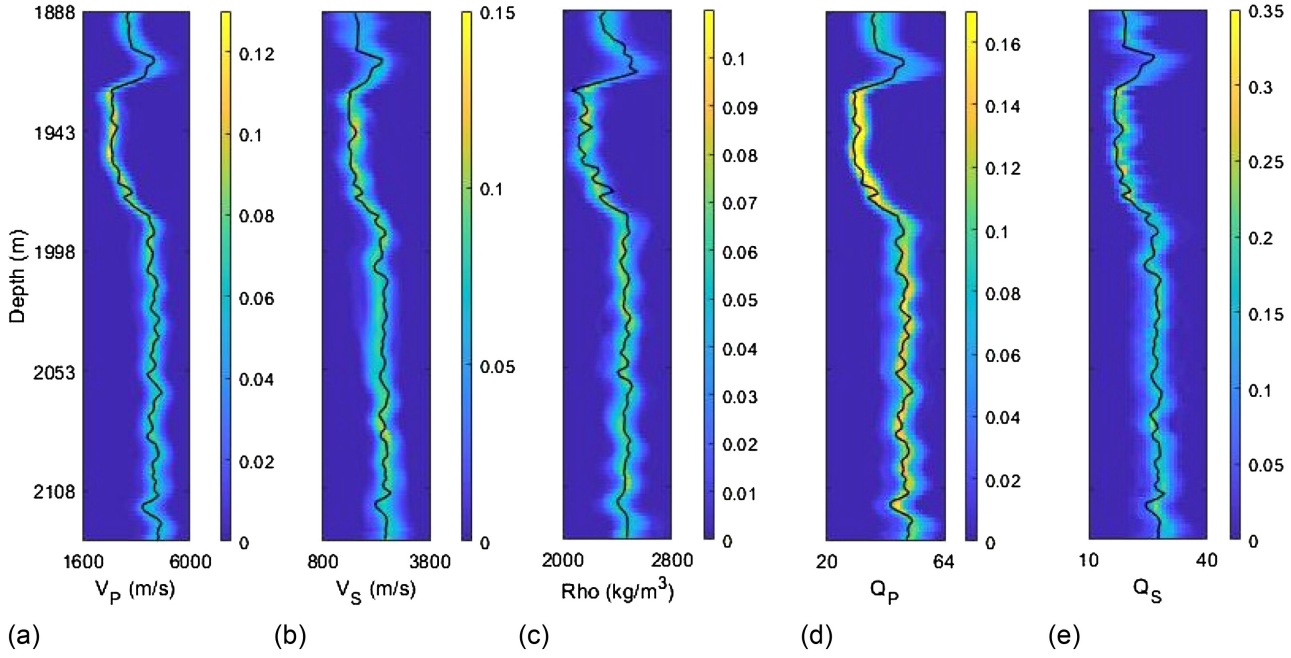

Figure 14. Inverted realizations of *P*-wave velocity (a), *S*-wave velocity (b), density (c), *P* (d) and *S* (e) wave quality factors.

the model variables with good convergence. The inversion process reliably estimates the fluid-related attenuation which demonstrates its effectiveness to be used as a direct fluid indicator. In the case of noisy data, the inversion results might show some instability and the solution might depend on the choice of the prior realization. In this case, we recommend the application of regularization parameters to obtain a stable estimation.

ACKNOWLEDGMENTS

We are grateful to the National IOR Centre of Norway led by the University of Stavanger for the financial support of this project. We would also like to acknowledge Lundin Energy Norway and their partners Wintershall Dea and OMW in the Edvard Grieg license for providing

the seismic data and well logs for this project. The computations and simulations were carried out with resources given by UNINETT Sigma2—the National Infrastructure for High-Performance Computing and Data Storage in Norway.

DATA AVAILABILITY

The synthetic data underlying this paper (example 1) will be shared on reasonable request to the corresponding author.

REFERENCES

Ahmed, N. & Weibull, W., 2022. Gradient descent optimization method for AVO inversion in viscoelastic media, in *Proceedings of the 83rd EAGE Annual Conference & Exhibition,* Vol. **2022,** pp. 1–5, European Association of Geoscientists & Engineers.

Ahmed, N., Khalid, P., Shafi, H. M.B. & Connolly, P., 2017. Dhi evaluation by combining rock physics simulation and statistical techniques for fluid identification of Cambrian-to-Cretaceous clastic reservoirs in Pakistan, *Acta Geophys.,* **65**(5), 991–1007.

Ahmed, N., Weibull, W.W. & Grana, D., 2022. Constrained non-linear AVO inversion based on the adjoint-state optimization, *Comput. Geosci.,* **168,** doi:10.1016/j.cageo.2022.105214.

Aki, K. & Richards, P.G., 2002. *Quantitative Seismology,* The Maple-Vail Book Manufacturing Group USA.

Aster, R.C., Borchers, B. & Thurber, C.H., 2018. *Parameter Estimation and Inverse Problems,* Elsevier.

Avseth, P., Mukerji, T. & Mavko, G., 2010. *Quantitative Seismic Interpretation: Applying Rock Physics Tools to Reduce Interpretation Risk,* Cambridge Univ. Press.

Buland, A. & Omre, H., 2003. Bayesian linearized AVO inversion, *Geophysics,* **68**(1), 185–198.

Carcione, J.M., 2007. *Wave Fields in Real Media: Wave Propagation in Anisotropic, Anelastic, Porous and Electromagnetic Media,* Elsevier.

Carcione, J.M. & Picotti, S., 2006. P-wave seismic attenuation by slow-wave diffusion: effects of inhomogeneous rock properties, *Geophysics,* **71**(3), O1–O8.

Caspari, E., Novikov, M., Lisitsa, V., Barbosa, N.D., Quintal, B., Rubino, J.G. & Holliger, K., 2019. Attenuation mechanisms in fractured fluid-saturated porous rocks: a numerical modelling study, *Geophys. Prospect.,* **67,** 935–955 .

Chapman, M., Liu, E. & Li, X.-Y., 2006. The influence of fluid sensitive dispersion and attenuation on AVO analysis, *J. geophys. Int.,* **167**(1), 89–105.

Chapman, S., Borgomano, J.V., Quintal, B., Benson, S.M. & Fortin, J., 2021. Seismic wave attenuation and dispersion due to partial fluid saturation: direct measurements and numerical simulations based on X-ray CT, *J. geophys. Res.,* **126**(4), e2021JB021643, doi:10.1029/2021JB021643.

Chen, H., Innanen, K.A. & Chen, T., 2018. Estimating P- and S-wave inverse quality factors from observed seismic data using an attenuative elastic impedance, *Geophysics,* **83**(2), R173–R187.

Cheng, G., Yin, X. & Zong, Z., 2020. Frequency-dependent spherical-wave nonlinear AVO inversion in elastic media, *J. geophys. Int.,* **223**(2), 765–776.

Cheng, G., Yin, X., Zong, Z., Xia, T., Wang, J. & Liu, H., 2022. Seismic inversion using complex spherical-wave reflection coefficient at different offsets and frequencies, *Geophysics,* **87**(2), R183–R192.

Cheng, W.-B., 2013. Three-dimensional seismic attenuation structure beneath the Taiwan region and its tectonic implication, *J. Asian Earth Sci.,* **65,** 86–99.

Cordua, K.S., Hansen, T.M. & Mosegaard, K., 2012. Monte Carlo full-waveform inversion of crosshole GPR data using multiple-point geostatistical a priori information, *Geophysics,* **77**(2), H19–H31.

de Figueiredo, L.P., Grana, D., Roisenberg, M. & Rodrigues, B.B., 2019. Gaussian mixture Markov Chain Monte Carlo method for linear seismic inversion, *Geophysics,* **84**(3), R463–R476.

Doyen, P., 2007. *Seismic Reservoir Characterization: An Earth Modelling Perspective,* Vol. **2,** EAGE Publications.

Dvorkin, J.P. & Mavko, G., 2006. Modeling attenuation in reservoir and nonreservoir rock, *Leading Edge,* **25**(2), 194–197.

Ehsan, M.I., Khalid, P., Ahmed, N., You, J., Liu, X. & Azeem, T., 2016. Seismic attenuation and velocity dispersion to discriminate gas hydrates and free gas zone, Makran offshore, Pakistan, *Int. J. Geosci.,* **7**(8), 1020–1028.

Fabien-Ouellet, G., Gloaguen, E. & Giroux, B., 2017. Time domain viscoelastic full waveform inversion, *J. geophys. Int.,* **209**(3), 1718–1734.

Grana, D., Mukerji, T. & Doyen, P., 2021. *Seismic Reservoir Modeling: Theory, Examples, and Algorithms,* John Wiley & Sons.

Grana, D., de Figueiredo, L. & Mosegaard, K., 2022. Markov chain Monte Carlo for petrophysical inversion, *Geophysics,* **87**(1), M13–M24.

Guo, G., Lan, H., Zhou, X., Liu, Y., Bin Waheed, U. & Chen, J., 2022. Topography-dependent eikonal tomography based on the fast-sweeping scheme and the adjoint-state technique, *Geophysics,* **87**(2), U29–U41.

Innanen, K.A., 2011. Inversion of the seismic AVF/AVA signatures of highly attenuative targets, *Geophysics,* **76**(1), R1–R14.

JafarGandomi, A. & Takenaka, H., 2013. Fdtd3c—a Fortran program to model multi-component seismic waves for vertically heterogeneous attenuative media, *Comput. Geosci.,* **51,** 314–323.

Jänicke, R., Quintal, B. & Steeb, H., 2015. Numerical homogenization of mesoscopic loss in poroelastic media, *Eur. J. Mech.-A/Solids,* **49,** 382–395.

Jänicke, R., Quintal, B., Larsson, F. & Runesson, K., 2019. Viscoelastic substitute models for seismic attenuation caused by squirt flow and fracture leak off, *Geophysics,* **84**(4), WA183–WA189.

Jin, Z., Chapman, M., Wu, X. & Papageorgiou, G., 2017. Estimating gas saturation in a thin layer by using frequency-dependent amplitude versus offset modelling, *Geophys. Prospect.,* **65**(3), 747–765.

Kamei, R. & Pratt, R., 2013. Inversion strategies for visco-acoustic waveform inversion, *J. geophys. Int.,* **194**(2), 859–884.

Keating, S. & Innanen, K.A., 2020. Parameter crosstalk and leakage between spatially separated unknowns in viscoelastic full-waveform inversion crosstalk analysis in viscoelastic FWI, *Geophysics,* **85**(4), R397–R408.

Khalid, P. & Ahmed, N., 2016. Modulus defect, velocity dispersion and attenuation in partially-saturated reservoirs of Jurassic sandstone, Indus basin, Pakistan, *Stud. Geophys. Geod.,* **60**(1), 112–129.

Kneib, G. & Shapiro, S.A., 1995. Viscoacoustic wave propagation in 2-D random media and separation of absorption and scattering attenuation, *Geophysics,* **60**(2), 459–467.

Kumar, D., Zhao, Z., Foster, D.J., Dralus, D. & Sen, M.K., 2020. Frequency-dependent AVO analysis using the scattering response of a layered reservoir, *Geophysics,* **85**(2), N1–N16.

Li, C. & Liu, X., 2019. Amplitude variation with incident angle inversion for q-factors in viscoelastic media: a case study, *Geophysics,* **84**(6), B419–B435.

Li, Q.-Z., 2017. *High-Resolution Seismic Exploration,* Society of Exploration Geophysicists.

Li, Y., Li, J., Chen, X., Zhang, J. & Bo, X., 2021. Prestack waveform inversion based on analytical solution of the viscoelastic wave equation prestack waveform inversion, *Geophysics,* **86**(1), R45–R61.

Liu, X., Greenhalgh, S., Kumar, M., Li, H., Liu, B., Liao, Q. & Huang, X., 2022. Reflection and transmission coefficients of spherical waves at an interface separating two dissimilar viscoelastic solids, *J. geophys. Int.,* **230**(1), 252–271.

Mavko, G., Dvorkin, J. & Walls, J., 2005. A theoretical estimate of S-wave attenuation in sediment, in *SEG Technical Program Expanded Abstracts 2005,* pp. 1469–1472, Society of Exploration Geophysicists.

Mavko, G., Mukerji, T. & Dvorkin, J., 2020. *The Rock Physics Handbook,* Cambridge Univ. Press.

Mosegaard, K. & Tarantola, A., 1995. Monte carlo sampling of solutions to inverse problems, *J. geophys. Res.,* **100**(B7), 12 431–12 447.
Nocedal, J. & Wright, S., 2006. *Numerical Optimization,* Springer Science & Business Media.
Operto, S., Gholami, Y., Prieux, V., Ribodetti, A., Brossier, R., Metivier, L. & Virieux, J., 2013. A guided tour of multiparameter full-waveform inversion with multicomponent data: from theory to practice, *Leading Edge,* **32**(9), 1040–1054.
Pan, W. & Wang, Y., 2020. On the influence of different misfit functions for attenuation estimation in viscoelastic full-waveform inversion: Synthetic study, *J. geophys. Int.,* **221**(2), 1292–1319.
Pan, W., Innanen, K.A. & Wang, Y., 2020. Seiselastic2D: an open-source package for multiparameter full-waveform inversion in isotropic-, anisotropic-and visco-elastic media, *Comput. Geosci.,* **145,** doi:10.1016/j.cageo.2020.104586.
Pang, S. & Stovas, A., 2020. Frequency-dependent pp and ps reflection coefficients in fractured media, *Geophys. Prospect.,* **68**(3), 926–940.
Peters, L., Anandakrishnan, S., Alley, R. & Voigt, D., 2012. Seismic attenuation in glacial ice: a proxy for englacial temperature, *J. geophys. Res.,* **117**(F2), doi:10.1029/2011JF002201.
Plessix, R.-E., 2006. A review of the adjoint-state method for computing the gradient of a functional with geophysical applications, *J. geophys. Int.,* **167**(2), 495–503.
Pride, S.R. & Berryman, J.G., 2003a. Linear dynamics of double-porosity dual-permeability materials. I. Governing equations and acoustic attenuation, *Phys. Rev. E,* **68**(3Pt 2), doi:10.1103/PhysRevE.68.036603.
Pride, S.R. & Berryman, J.G., 2003b. Linear dynamics of double-porosity dual-permeability materials. II. Fluid transport equations, *Phys. Rev. E,* **68**(3 Pt 2), doi:10.1103/PhysRevE.68.036604.
Pride, S.R., Berryman, J.G. & Harris, J.M., 2004. Seismic attenuation due to wave-induced flow, *J. geophys. Res.,* **109**(B1), doi:10.1029/2003JB002639.
Quintal, B., Schmalholz, S.M. & Podladchikov, Y.Y., 2009. Low-frequency reflections from a thin layer with high attenuation caused by interlayer flow, *Geophysics,* **74**(1), N15–N23.
Quintal, B., Steeb, H., Frehner, M. & Schmalholz, S.M., 2011. Quasi-static finite element modeling of seismic attenuation and dispersion due to wave-induced fluid flow in poroelastic media, *J. geophys. Res.,* **116**(B1), doi:10.1029/2010JB007475.
Sen, M.K. & Stoffa, P.L., 1996. Bayesian inference, Gibbs' sampler and uncertainty estimation in geophysical inversion, *Geophys. Prospect.,* **44**(2), 313–350.
Sen, M.K. & Stoffa, P.L., 2013. *Global Optimization Methods in Geophysical Inversion,* Cambridge Univ. Press.
Sheehan, A.F., de la Torre, T.L., Monsalve, G., Abers, G.A. & Hacker, B.R., 2014. Physical state of Himalayan crust and uppermost mantle: constraints from seismic attenuation and velocity tomography, *J. geophys. Res.,* **119**(1), 567–580.
Teng, L., Wang, S. & Cheng, J., 2012. Probabilistic petrophysical properties estimation integrating viscoelastic AVA inversion with statistical rock physics, in *Proceedings of the 2012 SEG Annual Meeting,* OnePetro.
Tisato, N. & Quintal, B., 2013. Measurements of seismic attenuation and transient fluid pressure in partially saturated Berea sandstone: evidence of fluid flow on the mesoscopic scale, *J. geophys. Int.,* **195**(1), 342–351.
Wang, W., McMechan, G.A. & Ma, J., 2021. Elastic isotropic and anisotropic full-waveform inversions using automatic differentiation for gradient calculations in a framework of recurrent neural networks, *Geophysics,* **86**(6), R795–R810.
Wang, Y., 2019. A constant-q model for general viscoelastic media, *J. geophys. Int.,* **219**(3), 1562–1567.
Waters, K.H. & Waters, K.H., 1981. *Reflection Seismology: A Tool for Energy Resource Exploration,* Wiley New York.
White, J., 1975. Computed seismic speeds and attenuation in rocks with partial gas saturation, *Geophysics,* **40**(2), 224–232.
White, J.E., Mihailova, N. & Lyakhovitsky, F., 1975. Low-frequency seismic waves in fluid-saturated layered rocks, *J. acoust. Soc. Am.,* **57**(S1), S30–S30.
Yang, J., Geng, J. & Zhao, L., 2020. A frequency-decomposed nonstationary convolutional model for amplitude-versus-angle-and-frequency forward waveform modeling in attenuative media, *Geophysics,* **85**(6), T301–T314.
Yong, P., Brossier, R. & Métivier, L., 2022. Parsimonious truncated newton method for time-domain full-waveform inversion based on the fourier-domain full-scattered-field approximation, *Geophysics,* **87**(1), R123–R146.
Zhao, H., Gao, J. & Liu, F., 2014. Frequency-dependent reflection coefficients in diffusive-viscous media, *Geophysics,* **79**(3), T143–T155.
Zong, Z., Yin, X. & Wu, G., 2015. Complex seismic amplitude inversion for p-wave and s-wave quality factors, *J. geophys. Int.,* **202**(1), 564–577.

APPENDIX A: ROCK PHYSICS MODELS FOR QUALITY FACTORS

The Waters empirical expressions (Waters & Waters 1981) in relation to *P*- and *S*-wave velocities V_P and V_S (expressed in km s^{-1}) are:

$$Q_P = 10.76 \times V_P, \qquad Q_S = 10.76 \times V_S. \tag{A1}$$

In the Dvorkin–Mavko nearly constant Q approximations, the formulation follows the wave-induced fluid flow (WIFF) mechanism and the order of magnitude of the *P*-wave seismic attenuation (inverse quality factor) is proportional to the contrast between relaxed and unrelaxed moduli (Mavko *et al.* 2020) as:

$$\frac{1}{Q_P} \approx \frac{M_\infty - M_0}{\sqrt{M_\infty M_0}}, \tag{A2}$$

where M_0 and M_∞ are the low frequency (relaxed) and high frequency (unrelaxed) limits of the compressional *P*-wave modulus M_P, respectively. The low-frequency limit (M_0) is obtained using Gassmann's fluid-substitution while the high-frequency limit (M_∞) is calculated using the patchy-saturation model (Mavko *et al.* 2020). The *P*-wave seismic attenuation depends on the difference between the two moduli. The *S*-wave seismic attenuation (Q_S^{-1}) is computed using a rock physics model for fully water-saturated rocks with heterogeneous solid frame (Dvorkin & Mavko 2006) as:

$$\left(\frac{Q_{P\text{-wet}}}{Q_{S\text{-wet}}}\right)^{-1} = \frac{5}{4}\frac{(\gamma-2)^2}{(\gamma-1)}\left(\frac{2\gamma}{3\gamma-2}\frac{\gamma}{3\gamma-3}\right)^{-1}, \qquad \gamma = \left(\frac{V_{P\text{-wet}}}{V_{S\text{-wet}}}\right)^2, \tag{A3}$$

where the subscript *wet* means that the rock is fully saturated with water and the attenuation depends on the spatial heterogeneity of the rocks. For fully water-saturated rocks, the low-frequency limit of the *P*-wave modulus is obtained as:

$$M_{0-\text{wet}} = \overline{M}_{\text{min}} \frac{\bar{\phi}\,\overline{M}_{\text{dry}} - (1+\bar{\phi})K_{\text{w}}\,\overline{M}_{\text{dry}}/\overline{M}_{\text{min}} + K_{\text{w}}}{(1-\bar{\phi})K_{\text{w}} + \bar{\phi}\,\overline{M}_{\text{min}} - K_{\text{w}}\,\overline{M}_{\text{dry}}/\overline{M}_{\text{min}}}, \tag{A4}$$

where $\bar{\phi} = \langle\phi\rangle$ and $\overline{M}_{\text{dry}} = \left\langle M_{\text{dry}}^{-1}\right\rangle^{-1}$ represent the arithmetic average of porosity and a harmonic average of dry-rock modulus and $\overline{M}_{\text{min}}$ and K_{w} are mineral and water moduli, respectively. The unrelaxed limit is computed as:

$$M_{\infty-\text{wet}} = \left\langle \left(M_{\text{min}} \frac{\phi\,M_{\text{dry}} - (1+\phi)K_{\text{w}}\,M_{\text{dry}}/M_{\text{min}} + K_{\text{w}}}{(1-\phi)K_{\text{w}} + \phi\,M_{\text{min}} - K_{\text{w}}\,M_{\text{dry}}/M_{\text{min}}} \right)^{-1} \right\rangle^{-1}. \tag{A5}$$

The *P*-wave seismic attenuation (Q_P^{-1}) is calculated from eq. (A2) by replacing the relaxed and unrelaxed moduli with $M_{0-\text{wet}}$ and $M_{\infty-\text{wet}}$. Finally, *P*- and *S*-wave velocities for water-saturated rocks ($V_{P-\text{wet}}$ and $V_{S-\text{wet}}$) are calculated using Gassmann's fluid substitution model by assuming the rock is fully saturated with water (Ahmed *et al.* 2017). The total attenuation is the sum of the two attenuation curves, that is the sum of the attenuation due to fluid and elastic heterogeneity in rock (Mavko *et al.* 2020).

Several studies (White 1975; White *et al.* 1975; Pride *et al.* 2004; Quintal *et al.* 2009, 2011; Tisato & Quintal 2013; Khalid & Ahmed 2016; Ehsan *et al.* 2016) demonstrate that the *P*-wave attenuation is frequency-dependent in partially saturated rocks due to wave-induced fluid flow (WIFF). Here, we use the analytical solution of White's 1-D interlayer-flow model (a 1-D WIFF model) given by Quintal *et al.* (2009) to estimate the frequency-dependent Q_P.

White's analytical solution (White 1975) for the interlayer-flow model describes the *P*-wave attenuation as frequency-dependent for a set of reservoir rock properties. Quintal *et al.* (2009) reformulated White's analytical solution as follows:

$$Q_{-\text{White}} = \frac{\text{Re}(b)}{\text{Im}(b)}, \tag{A6}$$

where Re and Im represent the real and imaginary parts while b is a complex number given by:

$$b = \left(1 + (I_1 g_1 + I_2 g_2)^{-1}\right)^{-1}. \tag{A7}$$

The complex *P*-wave modulus (H) is defined by the product of real numbers E_0 and b.

$$H = E_0 b, \tag{A8}$$

where

$$E_0 = \left(\frac{p_1}{E_{G1}} + \frac{p_2}{E_{G2}} \right)^{-1}. \tag{A9}$$

Indexes 1 and 2 describe the two different porous media and for each single saturated porous medium ($j = 1,2$). The equations are:

$$g_j = \frac{K_{Ej}}{2E_0(r_2 - r_1)^2 p_j}, \qquad I_j = \sqrt{i\omega' s_j}\,\coth\left(\frac{\sqrt{i\omega' s_j}}{2}\right), \qquad s_j = \frac{\eta_j d_j^2}{K_{Ej} k_j} \tag{A10}$$

$$p = \frac{d}{d_1 + d_2}. \tag{A11}$$

In the above equations, $\omega' = 2\pi f$, k and η are angular frequency, permeability and fluid viscosity while p and d refer to the saturation levels and layer thicknesses, respectively. The rest of the elastic properties (without index j) are given below and symbols are defined in Table 2.

$$E_G = K_{\text{sat}} + \frac{4}{3}\mu_d, \qquad K_E = \frac{E_d M}{E_G}, \qquad r = \frac{\beta_c M}{E_G} \tag{A12}$$

$$K_{\text{sat}} = K_d + \beta_c^2 M, \qquad \beta_c = 1 - \frac{K_d}{K_m}, \qquad M = \left[\frac{\beta_c - \phi}{K_m} + \frac{\phi}{K_f} \right]^{-1} \tag{A13}$$

and

$$E_d = K_d + \frac{4}{3}\mu_d. \tag{A14}$$

APPENDIX B: PARTIAL DERIVATIVES OF THE LAGRANGIAN

The derived partial derivatives of the Lagrangian of the misfit function are as follows:

$$\frac{\partial \mathcal{L}}{\partial V_P[i]} = \int_{\theta,\,\omega} \mathrm{d}\theta \left\{ \frac{A}{\alpha[i-1]}\ \lambda[i-1] - \frac{A}{\alpha[i]}\ \lambda[i] - \frac{A\Delta\alpha[i-1]}{2\alpha[i-1]^2}\ \lambda[i-1] - \frac{A\Delta\alpha[i]}{2\alpha[i]^2}\ \lambda[i] \right.$$
$$+ \frac{4\beta[i-1]^2}{\alpha[i-1]^3}\ \sin^2\theta\ \frac{\Delta\beta[i-1]}{\beta[i-1]}\ \lambda[i-1] + \frac{4\beta[i]^2}{\alpha[i]^3}\ \sin^2\theta\ \frac{\Delta\beta[i]}{\beta[i]}\ \lambda[i]$$
$$+ \frac{2\beta[i-1]^2}{\alpha[i-1]^3}\ \sin^2\theta\ \frac{\Delta\rho[i-1]}{\rho[i-1]}\ \lambda[i-1] + \frac{2\beta[i]^2}{\alpha[i]^3}\ \sin^2\theta\ \frac{\Delta\rho[i]}{\rho[i]}\ \lambda[i]$$
$$+ \frac{4}{\pi}\frac{\beta[i-1]^2}{\alpha[i-1]^3}\ \sin^2\theta\ \ln\left(\frac{\omega_o}{\omega'}\right)\ \frac{\Delta\Xi_S[i-1]}{\Xi_S[i-1]}\ \lambda[i-1]$$
$$\left. + \frac{4}{\pi}\frac{\beta[i]^2}{\alpha[i]^3}\ \sin^2\theta\ \ln\left(\frac{\omega_o}{\omega'}\right)\ \frac{\Delta\Xi_S[i]}{\Xi_S[i]}\ \lambda[i] \right\} \tag{B1}$$

$$\frac{\partial \mathcal{L}}{\partial V_S[i]} = \int_{\theta,\,\omega} \mathrm{d}\theta \left\{ -\frac{2\Delta\beta[i-1]}{\alpha[i-1]^2}\ \sin^2\theta\ \lambda[i-1] - \frac{2\Delta\beta[i]}{\alpha[i]^2}\ \sin^2\theta\ \lambda[i] \right.$$
$$- \frac{4\beta[i-1]}{\alpha[i-1]^2}\ \sin^2\theta\ \lambda[i-1] + \frac{4\beta[i]}{\alpha[i]^2}\ \sin^2\theta\ \lambda[i]$$
$$- \frac{2\beta[i-1]}{\alpha[i-1]^2}\ \sin^2\theta\ \frac{\Delta\rho[i-1]}{\rho[i-1]}\ \lambda[i-1] - \frac{2\beta[i]}{\alpha[i]^2}\ \sin^2\theta\ \frac{\Delta\rho[i]}{\rho[i]}\ \lambda[i]$$
$$+ \frac{4}{\pi}\frac{\beta[i-1]}{\alpha[i-1]^2}\ \sin^2\theta\ \ln\left(\frac{\omega_o}{\omega'}\right)\ \frac{\Delta\Xi_S[i-1]}{\Xi_S[i-1]}\ \lambda[i-1]$$
$$\left. + \frac{4}{\pi}\frac{\beta[i]}{\alpha[i]^2}\ \sin^2\theta\ \ln\left(\frac{\omega_o}{\omega'}\right)\ \frac{\Delta\Xi_S[i]}{\Xi_S[i]}\ \lambda[i] \right\} \tag{B2}$$

$$\frac{\partial \mathcal{L}}{\partial \rho[i]} = \int_{\theta} \mathrm{d}\theta \left\{ C[i-1]\left(\frac{1}{\rho[i-1]}\right)\ \lambda[i-1] - C[i]\left(\frac{1}{\rho[i]}\right)\ \lambda[i] - C[i-1]\left(\frac{\Delta\rho[i-1]}{\rho[i-1]^2}\right)\ \lambda[i-1] - C[i]\left(\frac{\Delta\rho[i]}{\rho[i]}\right)\ \lambda[i] \right\} \tag{B3}$$

$$\frac{\partial \mathcal{L}}{\partial \xi_P[i]} = \int_{\theta,\,\omega} \mathrm{d}\theta \left\{ \frac{D}{\Xi_P[i-1]}\ \lambda[i-1] - \frac{D}{\Xi_P[i]}\ \lambda[i] - \frac{D}{2}\ \frac{\Delta\Xi_P[i-1]}{\Xi_P[i-1]^2}\ \lambda[i-1] + \frac{D}{2}\ \frac{\Delta\Xi_P[i]}{\Xi_P[i]^2}\ \lambda[i] \right\} \tag{B4}$$

and

$$\frac{\partial \mathcal{L}}{\partial \xi_S[i]} = \int_{\theta,\,\omega} \mathrm{d}\theta \left\{ \frac{E}{\Xi_S[i-1]}\,\lambda[i-1] - \frac{E}{\Xi_S[i]}\,\lambda[i] - \frac{E}{2}\ \frac{\Delta\Xi_S[i-1]}{\Xi_S[i-1]^2}\,\lambda[i-1] - \frac{E}{2}\ \frac{\Delta\Xi_S[i]}{\Xi_S[i]^2}\ \lambda[i] \right\}. \tag{B5}$$

The state variable λ is given by the equation as:

$$\lambda[i] = -\sum_{\omega'=1}^{p} W(\omega') * (d[i] - f[i])(\hat{\omega}).\delta(\omega' - \hat{\omega}). \tag{B6}$$